small methods
www.small-methods.com

A Microcavity Chemiluminescent Immunoimaging Protocol for Fast in Situ Detection of Antibody Secreted from Single Hybridoma Cells

Hang Ao, Wencheng Xiao, Weiwei Chen, Wenrui Hu, Jie Wu, and Huangxian Ju**

Chemiluminescent immunoassay is the most widely used protein detection technique in clinical diagnosis but still faces substantial challenges in antibody-related single-cell analysis due to the lack of a homogeneous immunoassay with strong and stable chemiluminescence signal. Herein, a single-cell microfluidic platform for efficient in situ detection of antibody secreted from single hybridoma cells through a microcavity chemiluminescent immunoimaging (MCCLII) protocol is reported, which consist of an imidazole-enhanced chemiluminescence system, a proximity-triggered DNA nanomachine and a hybrid-regulated hemin-DNA switch. In MCCLII, antibody secreted from single hybridoma cells can be visualized through a homogeneous proximity CL assay, which converses the target antibody to DNA for triggering the DNA nanomachine and then activates the catalytic activity of hemin-DNA switch to produce strong and persistent chemiluminescence for micro-imaging. The MCCLII realizes immunoimaging detection down to 66 antibody molecules in 0.79-nL microchamber and demonstrates the possibility of specific hybridoma cell screening within 30 min, which provides a simple and fast antibody screening platform to promote antibody-drug production.

1. Introduction

Monoclonal antibodies (mAbs) are one of the most utilized biomolecules for cancer therapy.[1] However, the widely used hybridoma technology for the discovery of mAbs is still unable to satisfy the growing demand for high-throughput production of specific antibodies due to the low efficiency of specific hybridoma cell screening.[2] Recently, microfluidic methods raise the interests of scientists and gradually become a powerful platform for discovery of mAbs.[3] Through the in situ detection of the antibody secreted from single hybridoma cells in a restricted atmosphere, specific hybridoma cells with high activity can be sorted. Although a series of fluorescence (FL) assays have been developed for the screening of specific hybridoma cells on microdroplet-based chips,[4] the need of specialized molecular probes, the difficulty in adding reagents and washing, the insufficient sensitivity for fast screening of hybridoma cells and the usage of extremely expensive equipment hinder the wide use of micro-platform. Chemiluminescence (CL) imaging technique has attracted wide attention due to its advantages of low background, high sensitivity, simple instrument and low cost for bioimaging analysis.[5] The CL array-based imaging assays can achieve the high-throughput requirements of single cell analysis,[6] which makes CL imaging technique a good candidate for the lab-on-chip screening of specific hybridoma cells. Unfortunately, the commonly used heterogeneous imaging assays based on horseradish peroxidase (HRP)-luminol-H_2O_2 CL system suffer from the complex interface modification and tedious washing steps to ensure the optimal signal-to-noise ratio,[7] are thus difficult to be perform in microfluidic chips. The development of homogeneous CL imaging assays with high sensitivity is still a challenge for the lab-on-chip single cell analysis.

To overcome the limitations of natural HRP-based heterogeneous CL assays, various peroxidase-mimicking enzymes have been developed.[8] The peroxidase mimic DNAzyme G-quadruplex/hemin (G4/hemin) complex is commonly used for developing homogeneous CL imaging assays.[9] However, the requirement for a specific sequence in G4/hemin, and the poor solubility and self-aggregation of hemin limit the application of G4/hemin-based CL switch for wide target detection.[10] Our research group previously developed several FL switches based on the hemin labelled oligonucleotide (hemin-DNA), which improved the stability of hemin and could be easily used to establish homogeneous switch of hemin activity through the hybridization of hemin-DNA with target sequence.[11] However, the CL signal

H. Ao, W. Xiao, W. Hu, J. Wu, H. Ju
State Key Laboratory of Analytical Chemistry for Life Science
School of Chemistry and Chemical Engineering
Nanjing University
Nanjing 210023, China
E-mail: wujie@nju.edu.cn; hxju@nju.edu.cn
W. Chen
State Key Laboratory of Flexible Electronics
School of Chemistry and Life Sciences
Nanjing University of Posts and Telecommunications
Nanjing 210023, China

The ORCID identification number(s) for the author(s) of this article can be found under https://doi.org/10.1002/smtd.202500656

DOI: 10.1002/smtd.202500656

produced from hemin-DNA catalyzed luminol-H_2O_2 system is not strong enough for practical applications of CL imaging assays on microchips, and the flash-type CL signal of luminol-H_2O_2 CL system is not conductive to the microfluidic operation on a microchip,[12] which leads to the false negatives. Therefore, the enhancements of both signal intensity and stability of hemin-DNA-based CL system become the primary barrier for the successful implementation of the hemin-DNA switch in CL microimaging assay.

Inspired by the natural HRP structure, some researchers have utilized histidine and its analogue to modify G4 or oligopeptides for significantly enhancing the catalytic activity of hemin.[13] In this work, we discovered an imidazole (Im)-enhanced hemin-DNA switch-L012-H_2O_2 system, designed a proximity-triggered DNA nanomachine (DNM), and proposed a microcavity chemiluminescent immunoimaging (MCCLII) protocol for the detection of single hybridoma cell secreted antibody on a microchip. The designed microchip enabled the capture of a single hybridoma cell in a microcavity along with the CL detection set, which consisted of a pair of affinity probes, an iblock/initiator, the designed DNM and activity-inhibited double strand hemin-DNA probes. The in situ secreted monoclonal antibody from the captured hybridoma cells could be visualized through the immunological recognition of target antibody by affinity probes, which induced the release of initiator and then triggered the DNM to open the hemin-DNA switch for the generation of strong and long-lasting CL signal. The proposed MCCLII protocol for anti-PCSK9-antibody showed a detection limit of 5.67 pg mL^{-1} in 96-well plate, and could achieve in situ immunoimaging detection of 66 antibodies secreted from single hybridoma cells on the microchip, and specific hybridoma cell screening within 30 min, providing a powerful method for the discovery and high-throughput production of specific mAbs.

2. Results and Discussion

2.1. Chemiluminescent Micro-Imaging Assay Strategy for Specific Hybridoma Cell Screening

In order to achieve the rapid screening of specific hybridoma cells, a MCCLII protocol on a microchip was first developed for in situ detection of single hybridoma cell-secreted antibody. As shown in **Figure 1a**, Im was introduced to enhance the CL intensity of hemin-DNA-L012-H_2O_2 system via enhancing hemin activity and reducing reaction energy of L012 oxidation. As for the CL detection of single hybridoma cell-secreted antibody on microchip, a proximity binding-triggered DNM-regulated hemin-DNA switch was designed (Figure 1b). A single hybridoma cell was encapsulated in a microcavity along with CL detection reagents, which contained a pair of affinity probes, an iblock/initiator complex, a designed DNM and activity-inhibited hemin-DNA probe. The in situ secreted antibody from the captured hybridoma cell could be immuno-recognized by a pair of affinity probes to form a proximity complex, which contained a newly assembled sequence to hybridize with iblock in the iblock/initiator complex for releasing the initiator. The released initiator then triggered the cascade strand displacement reaction of the DNM along the DNA skeleton to produce a large number of primers for opening the hemin-DNA switch, which separated the inactivated hemin-DNA dimer into highly active hemin-DNA monomer. After the addition of CL substrates, CL dot signal could be observed in the microcavity with a specific hybridoma cell for the screening of specific hybridoma cells with high secretion ability.

2.2. Mechanism of Hemin-DNA Switch-L012-H_2O_2 CL System Enhanced by Im

The kinetic curve of hemin-L012-H_2O_2 system exhibited a weak and quickly decreased CL signal, while a strong and long-lasting CL phenomenon was observed in hemin-DNA-L012-H_2O_2 system (Figure S1, Supporting Information), here D1 was used for the preparation of hemin-DNA (Table S1, Supporting Information), which could be attributed to the high stability of hemin-DNA due to the linkage of hemin with oligonucleotide.[14] Therefore, hemin-DNA was employed as the catalyst for further constructing the CL detection protocol.

Several small molecular reagents were used to evaluate their effects to the CL performance of the hemin-DNA-L012-H_2O_2 system (Figure S2, Supporting Information), among which Im exhibited the best performance to enhance the CL signal (**Figure 2a**), thus Im was utilized as the enhancer of hemin-DNA-L012-H_2O_2 system. The UV–vis absorption spectrum of hemin-DNA showed a Soret absorption band centered at 401 nm for the hemin moiety (Figure S3, Supporting Information). A red shift of the absorption band was observed in the presence of Im, indicating the axial coordination between Im and hemin moiety.[15] The effect of Im on hemin-DNA activity was assessed with both colorimetric method using 3,3′,5,5′-tetramethylbenzidine (TMB) as the substrate and CL method using L012 as the emitter, respectively. The initial velocity (v_0) of TMB oxidation in the absence and presence of Im exhibited a slight enhancement of Im on catalytic activity in hemin-DNA-TMB-H_2O_2 system (Figure 2b) due to the coordination between Im and hemin moiety, which led to a significant CL enhancement of hemin-DNA-L012-H_2O_2 system (Figure 2c), indicating that Im possessed greater influence on L012 oxidation.

After Im was introduced into hemin-DNA-TMB-H_2O_2 system, both the Michaelis constant K_m and the maximum velocity v_{max} increased (Table S2, Supporting Information), suggesting that Im could enhance the flexibility of hemin moiety but decrease the affinity of hemin moiety to TMB. In contrast, the introduction of Im decreased the K_m value and sharply increased v_{max} of hemin-DNA-L012-H_2O_2 CL system (Figure S4, Supporting Information), which implied that Im could simultaneously enhance the affinity of hemin moiety to L012 and the flexibility of hemin moiety to improve the CL emission, as shown in Figure 1a.

The Im-enhanced hemin-DNA-L012-H_2O_2 system showed a long-lasting CL emission (Figure 2d). After the addition of H_2O_2 to the mixture of hemin-DNA and L012, a weak and glowing-type CL signal was observed. The subsequent addition of Im caused a sharp increasing of CL intensity and maintained the long-lasting CL phenomenon. This result suggested that Im facilitated the production of more active substrates in the presence of highly active hemin moiety. Notably, the Im-assisted CL enhancement could be observed in a wide pH range and can be applied to both hemin and the hemin-DNA catalyzed

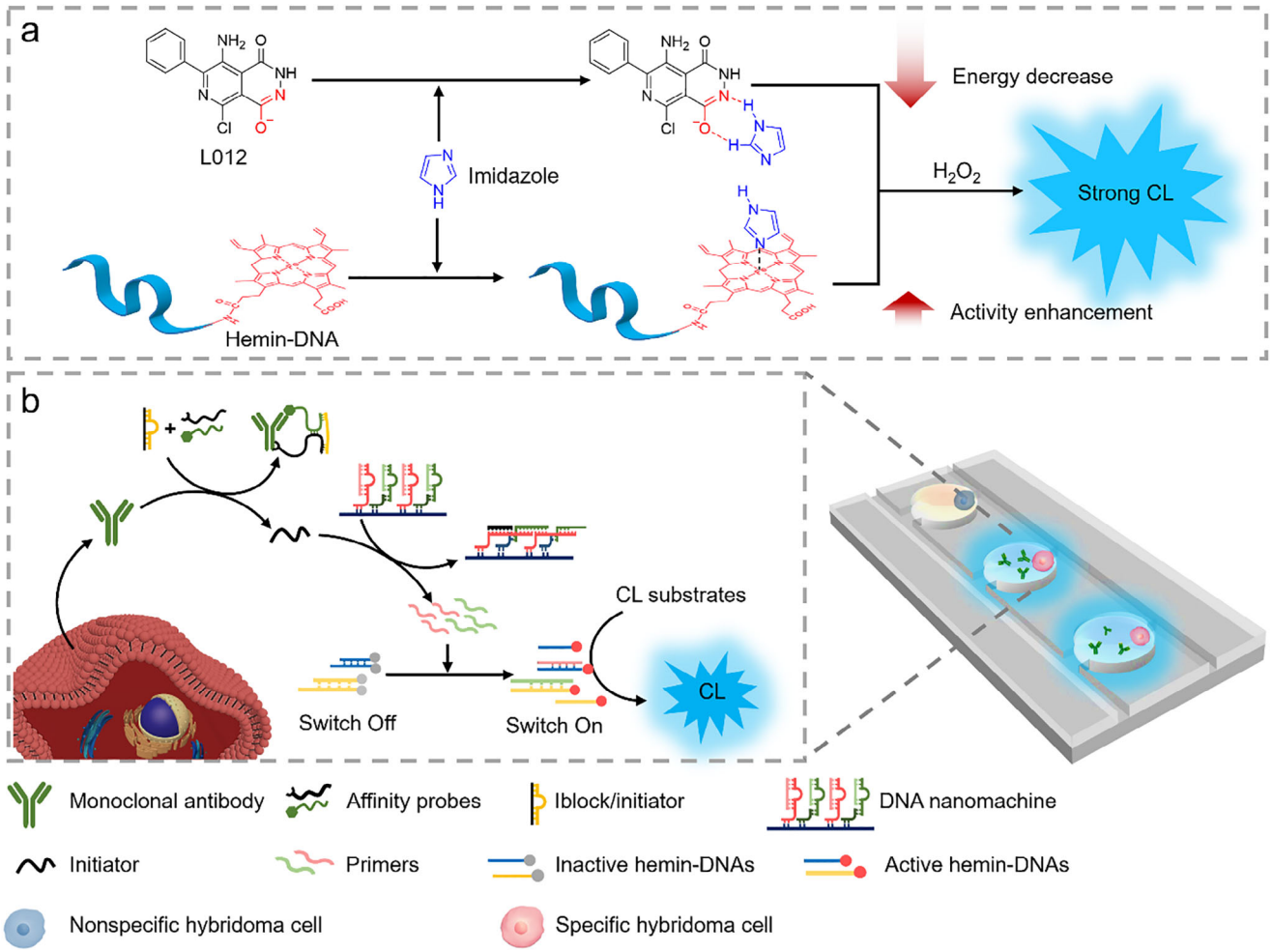

Figure 1. a) Schematic illustration of Im-enhanced hemin-DNA-L012-H_2O_2 CL system via activating the hemin and reducing the reaction energy of L012 oxidation. b) Schematic illustration of MCCLII for in situ detection of antibody secreted from single hybridoma cell loaded on a microchip.

L012-H_2O_2 system (Figure S5, Supporting Information), implying that Im could serve as a common CL enhancer of hemin-related CL system.

Azoles have been proved to be efficient organocatalysts for transamidation reaction through the formation of two hydrogen bonds to decrease the reaction energy of the nucleophilic reaction between a carboxamide and an amine.[16] Thus it was reasonable to hypothesize that L012-based CL reaction involved the nucleophilic reaction of the carboxamide moiety in L012 (Figure 2e),[17] and that Im could decrease the reaction energy through the formation of hydrogen bonds between Im and L012. The process of Im-assisted L012 oxidation was proposed in Figure 2f. Different from the direct nucleophilic attack of oxygen species to L012 (blue arrow), Im was first connected with L012 through two hydrogen bonds (B0), and then reactive oxygen species attacked the carboxamide moiety to break the -C-N- bond (red arrow), which led to a significant downfield shift of the peak of NH^1 proton in L012 upon the presence of Im (Figure S6, Supporting Information), which could be attributed to the reduction of the electron density of NH^1 proton on L012 due to the hydrogen bond formation.[18] DFT calculations were performed to further prove the reaction process of the Im-assisted L012 oxidation. The activation barrier for L012 oxidation was found to be decreased from 1.29 to 0.91 eV upon the introduction of Im (Figure 2g), which implied that Im could facilitate the L012 oxidation by reducing the reaction energy. Therefore, it could be concluded that Im assisted the oxidation of L012 via enhancing the enzyme activity of hemin moiety and reducing the reaction energy of L012 to produce strong and long-lasting CL signal.

In order to investigate the effect of DNA sequence in hemin-DNA on the CL enhancement of Im, four different hemin-DNAs (hemin-D1, hemin-D2, hemin-D3 and hemin-D4) were used to catalyse the CL reaction of L012-H_2O_2 system, which exhibited different initial CL intensity, but all four hemin-DNA showed significant CL signal enhancement in the presence of Im (Figure S7, Supporting Information), indicating that DNA sequence in hemin-DNA only affected the catalytic ability of hemin-moiety, did not significantly change the Im-assisted L012 oxidation.

The effects of other azoles were also evaluated, and 1,2,4-triazole (Tz) was also found to exhibit the significantly enhanced CL performance (Figure 2h). Similar to Im, its effect

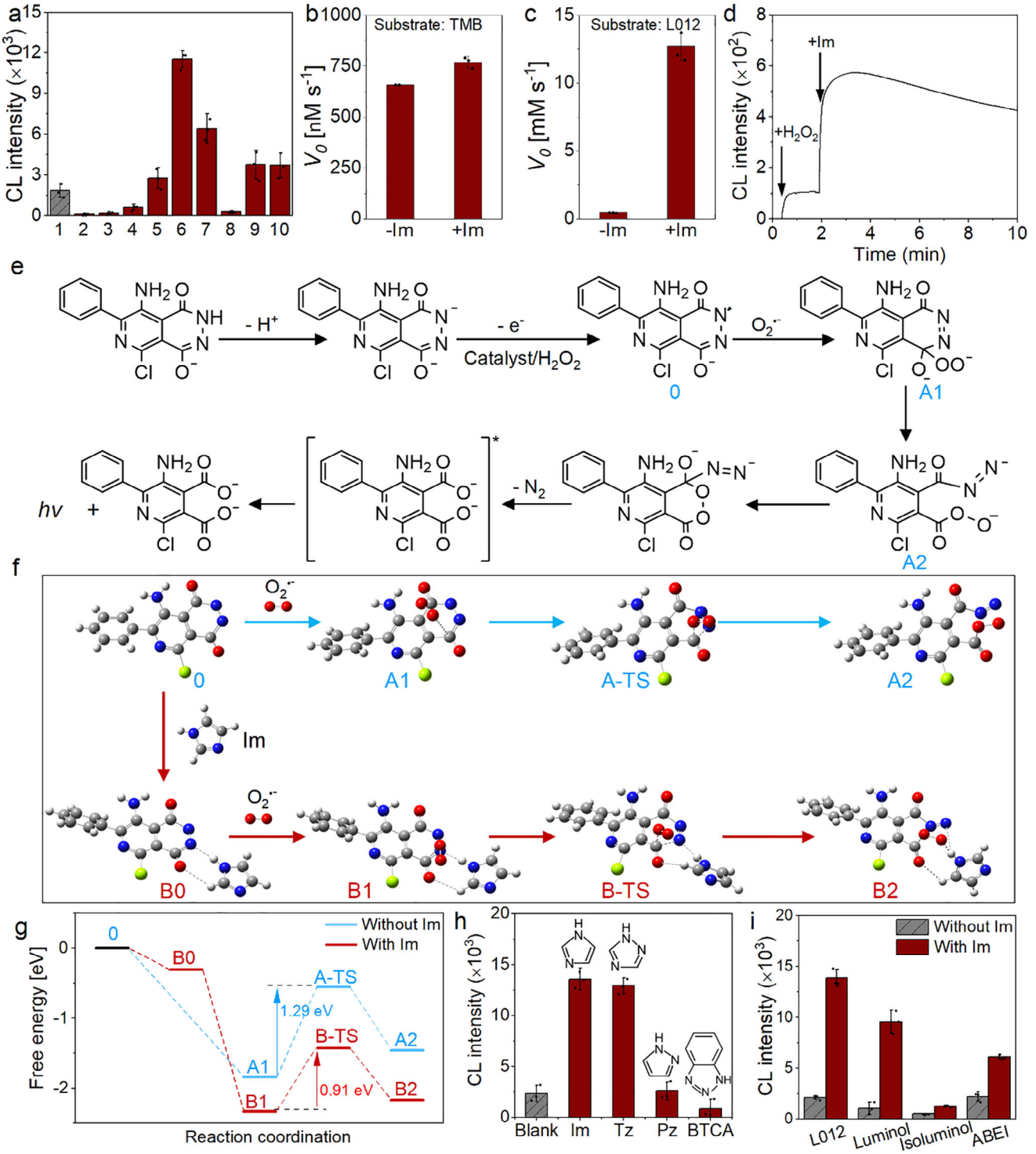

Figure 2. a) CL intensity of 10 mM pH 7.2 PBS containing 0.1 mM L012, 1 mM H_2O_2, and 20 nM hemin-D1 in absence (column 1) and presence of 4 mM PIP, 4-chlorothiophenol, 1,4-NTPA, tryptophan, Im, 2-MIM, ICA, MICA or His (columns 2 to 10). Catalytic activity of hemin-DNA for b) TMB and c) L012 oxidation in absence and presence of Im. d) Change in CL kinetic curve of 10 mM pH 7.2 PBS containing 0.1 mM L012 and 20 nM hemin-D1 upon consecutive addition of 1 mM H_2O_2 and 4 mM Im. e) General CL mechanism of L012 oxidation by superoxide radical in aqueous solution. f) DFT calculation of L012 oxidation and Im-enhanced L012 oxidation. g) Energy profiles along the pathways for L012 oxidation in absence and presence of Im. h) CL intensity of 10 mM pH 7.2 PBS containing 0.1 mM L012, 1 mM H_2O_2, and 20 nM hemin-D1 in presence of 4 mM Im, Tz, Pz or BTCA. i) CL intensity of 10 mM pH 7.2 PBS containing 1 mM H_2O_2, 20 nM hemin-D1 and 0.1 mM L012, luminol, isoluminol or ABEI in the absence and presence of 4 mM Im. Error bars: mean ± SD, $n = 3$.

on the colorimetric reaction of hemin-DNA-TMB-H_2O_2 system was much weaker than the CL reaction of hemin-DNA-L012-H_2O_2 (Figure S8a,b, Supporting Information). However, the CL enhancement of Tz on hemin-DNA-L012-H_2O_2 system exhibited a relatively faster decay than Im (Figure S8c, Supporting Information). Moreover, Tz did not change the absorption peak of the hemin moiety in both absorbance and the wavelength (Figure S8d, Supporting Information), while the intensity of L012 absorbance slightly decreased in the presence of Tz (Figure S8e, Supporting Information), indicating that Tz had no impact on hemin-DNA but affect L012 structure. The effects of Tz on K_m values and v_{max} of both hemin-DNA-TMB-H_2O_2 and hemin-DNA-L012-H_2O_2 CL system were also examined, which showed the changes similar to those of Im (Table S2 and Figure S4, Supporting Information), indicating the similar enhancement of Im on the flexibility of hemin moiety and the affinity of L012. The lower K_m and v_{max} in the presence of Tz than Im implied the greater decrease of CL reaction energy of L012 in the presence of Im. Therefore, it could be concluded that Im was a better enhancer of hemin-DNA-L012-H_2O_2 CL system. More interestingly, Im was also the most efficient enhancer of L012 or luminol oxidation compared to other CL substrates such as isoluminol and N-(4-aminobutyl)-N-ethylisoluminol (ABEI) (Figure 2i), further demonstrating the suggested enhancement mechanism of Im on hemin-DNA-L012-H_2O_2 CL system.

The effect of Im on the CL performance of HRP catalyzed CL system was also evaluated., The addition of imidazole did not enhance the CL signal of HRP catalyzed L012-H_2O_2 CL system (Figure S9, Supporting Information), indicating that imidazole could be used as a CL enhancer only for the hemin-based CL system.

2.3. Enzymatic Activity Regulated CL Switch and Initiator-Activated DNA Nanomachine for CL imaging

Different from G4/hemin DNAzyme, which is commonly sequence-dependent, hemin-DNA activity regulative strategy provides another approach to design the CL switch through a simple strand displacement reaction to separate the inactive hemin-DNA dimer into two high activity hemin-DNA monomers (**Figure 3a**).[11] Moreover, the enhancement of Im on hemin-DNA-L012-H_2O_2 CL system was more efficient compared to that of G4/hemin-L012-H_2O_2 CL system (Figure 3b). Besides, G4/hemin catalyzed L012-H_2O_2 CL system showed a flash-type CL emission, whereas the hemin-DNA switch exhibited a long-lasting CL emission after the hemin-DNA switch was turned on with a primer (Figure 3c). The CL images of hemin-DNA switch also exhibited a slow derease of the CL signal (Figure S10, Supporting Information), indicating the stability of hemin-DNA catalyzed L012-H_2O_2 CL system over the measuement window in both 96-well plate and microchip. Thus, this robust and persistent CL signal of Im-enhanced hemin-DNA-L012-H_2O_2 system was used for homogeneous CL imaging detection on microchips.

To gain the best performance of primer regulated hemin-DNA switch, the detection conditions including pH, concentrations of Im, H_2O_2 and L012 were optimized. At pH 7.2 the Im-enhanced hemin-DNA-L012-H_2O_2 CL system showed the highest CL intensity and signal-to-noise ratio (Figure S11a, Supporting Information), thus it was considered to be a suitable pH condition for homogeneous detection of in situ secreted antibody of hybridoma cell on microchips. Similarly, the maximum signal-to-noise ratios were observed at 4 mM Im, 1 mM H_2O_2 and 0.1 mM L012, respectively (Figure S11b–d, Supporting Information), which were used as the conditions for further CL imaging.

For realizing the highly sensitive detection of single hybridoma cell secretion using the hemin-DNA switch, the initiator-activated DNA nanomachine (DNM) was designed through alternate hybridization of C1 (block-1/primer-1) and C2 (block-2/primer-2) on a DNA skeleton to amplify the signal of target antibody (Figure 3d). Under the presence of initiator, its hybridization with block-1 from C1 opened the bulge loop of block-1 and released primer-1, the exposed bulge loop of block-1 subsequently opened the bulge loop of block-2 from C2 to release primer-2, and the exposed bulge loop of block-2, which contained the same sequence with the initiator, then initiated another hybridization reaction between C1 and C2 (Figure S12, Supporting Information). Thus, a cascade hybridization reaction occurred along the DNA skeleton with high local concentration to realize the rapid DNA amplification for releasing abundant primers to activate the hemin-DNA switch.

In order to obtain the best performance of initiator-triggered DNM, the number of complementary bases at the 5′ end of block-1 with primer-1 was optimized by CL imaging, and the initiator-triggered primer release was verified by FL method (Figure S13a, Supporting Information). The CL background of hemin- DNA switch decreased with the increasing number of complementary bases (Figure S13b, Supporting Information), implying that the 5′ end of block-1 could hybridize well with the 3′ end of primer-1 for the blocking of primer-1 to prevent the non-specific background signal. The maximum signal-to-noise ratio was obtained when 7 bases of 5′ end of block-1 was hybridized with the 3′ end of primer-1, which led to the strongest FL signal when the primer-1′ was labeled with a FAM moiety (Figure S13c, Supporting Information). However, when block-1′ with 7 pairs of complementary bases at the 5′ end was used to hybridized with primer-1′ to form C1', the FL signal sharply decreased due to the approach of FAM to BHQ, implying the successful hybridization of the 3′ end of primer-1′ with the 5′ end of block-1′. Upon the addition of initiator, the FL signal recovered to the original intensity of primer-1′, indicating the excellent release efficiency of primer-1′. Thus, the 7 pairs of complementary bases were chosen for the fabrication of C1 and C2.

The assembly of DNM was verified by gel electrophoresis (Figure S14, Supporting Information). After primer-1 hybridized to block-1 and primer-2 to block-2, the corresponding hybridization products C1 and C2 exhibited single bands with relatively slow migration (lanes 7 and 8). After the assembly of DNM, a band with much slower migration (lane 10) was observed, which indicated the successful synthesis of DNM. The feasibility of the cascade DNA reaction between C1 and C2 was also verified by PAGE (Figure S15, Supporting Information). After mixing C1 and C2, their DNA bands did not obviously change (lane 3). However, multiple bands at high molecule weight appeared after the addition of a small amount of initiator (20 nM), and a new band appeared at low molecule weight (lane 4), indicating the cascade hybridization reaction between C1 and C2 and the release of primers.

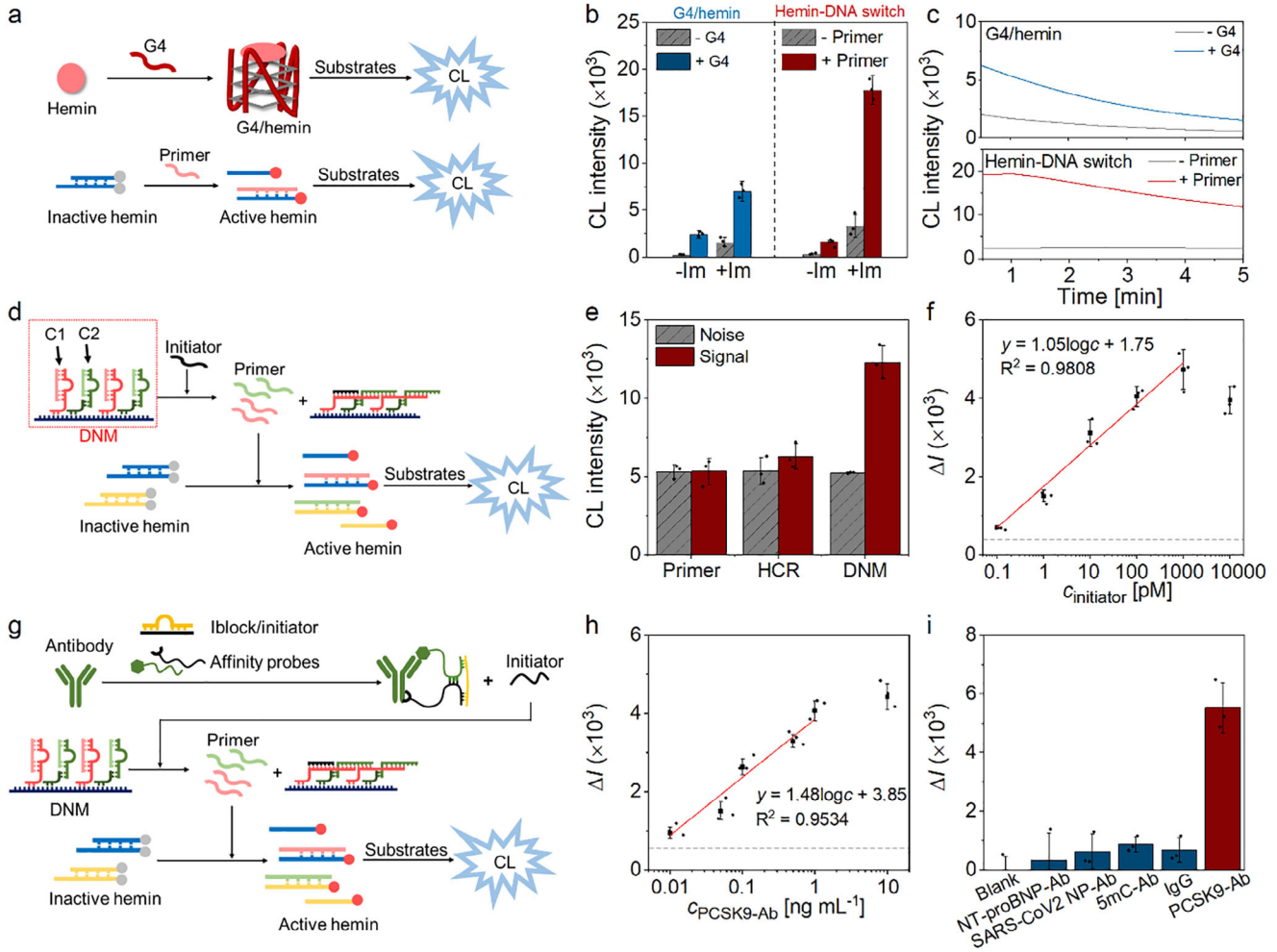

Figure 3. a) Schematic diagram of CL responses based on G4/hemin or hemin-DNA switch. b) CL intensity and of G4/hemin-L012-H_2O_2 and hemin-DNA switch-L012-H_2O_2 systems in absence and presence of Im. c) dynamic curves of G4/hemin-L012-Im-H_2O_2 systems with and without G4, and dynamic curves of hemin-DNA switch-L012-Im-H_2O_2 system with and without primer. The CL intensity is collected every 30 s, with a total of 10 data points for each sample within 5 min. d) Schematic diagram of initiator-triggered DNM for activating the CL system of hemin-DNA switch-L012-H_2O_2. e) CL intensity of hemin-DNA switch-L012-H_2O_2 system in absence (noise) and presence (signal) of 1 nM primer-1, and HCR or DNM products activated by 1 nM initiator. f) Plot of relative CL signal of hemin-DNA switch-L012-H_2O_2 system versus initiator concentration. g) Schematic diagram of antibody-triggered DNM for activating the CL system of hemin-DNA switch-L012-H_2O_2. h) Relative CL signal of DMEM containing 0.1 mM L012, 1 mM H_2O_2, 4 mM Im, 20 nM hemin-D1/D2-hemin, 20 nM hemin-D3/D4-hemin, 40 nM DNM, 20 ng mL^{-1} PCSK9-P1, 20 ng mL^{-1} Ab2-P2 and 20 nM iblock/initiator as logarithm function of PCSK9-Ab concentration. i) Specificity of the proposed CL assay at 1 ng mL^{-1} NT-proBNP-Ab, SARS-CoV2 NP-Ab, 5mC-Ab, IgG, and PCSK9-Ab. Error bars: mean ± SD, $n = 3$.

2.4. Chemiluminescent Response to Initiator and PCSK9-Ab

The CL signal of DNM-activated hemin-DNA switch exhibited the time-dependent increase after the addition of initiator, and reached the maximum signal at 20 min (Figure S16, Supporting Information). Thus, the incubation time of 20 min was used for activating the DNM, at which the initiator-triggered hybridization chain reaction (HCR) between C1 and C2 produced only slight CL signal, close to the background and that without any amplification (Figure 3e). However, the initiator-triggered DNM could activate hemin-DNA switch to generate a strong CL signal at a low concentration of initiator in a short time. This efficient signal amplification was benefited from the high local concentration of reactants, which were confined on the DNA skeleton, leading to the acceleration of reaction kinetics and improvement of reaction efficiency. This DNM enabled the rapid and sensitive detection of initiator-related target. Here, the CL signal exhibited a logarithmic increase with the increasing concentration of initiator within a linear range from 0.1 pM to 1 nM (Figure 3f). This result guaranteed the feasibility of quantitative analysis for protein detection through DNM-activated hemin-DNA switch combined with proximity binding-induced initiator release.

A proximity induced DNA assembly[19] was used for CL assay of antibody through the proximity binding-triggered DNM to activate hemin-DNA switch-L012-H_2O_2 CL system (Figure 3g). The target antibody was first specifically recognized by a pair of affinity probes to form a new sequence, which hybridized with the iblock to release the initiator from iblock/initiator. The

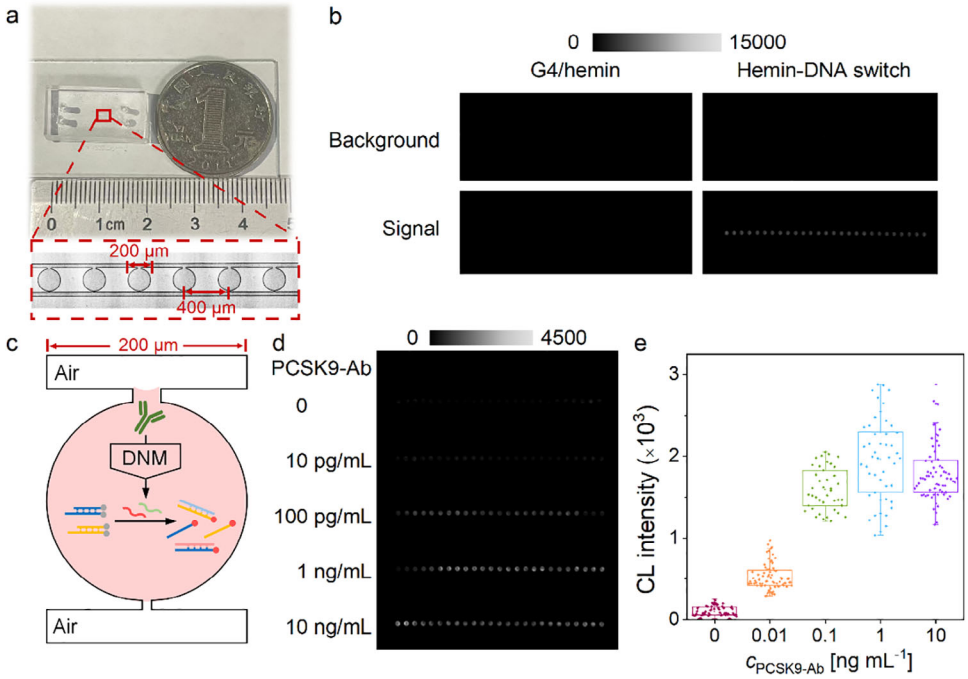

Figure 4. a) Photograph of designed microchip with a Chinese one-yuan coin, and micro-image of 6 microchambers in the microchip containing 25 microchambers. b) CL images of Im-enhanced G4/hemin- and hemin-DNA switch-L012-H_2O_2 system in absence (background) and presence of G4 or primer-1 (signal) in the microchip. c) Schematic diagram of specific monoclonal antibody detection in single microcavity. d) CL images and e) CL intensities of DMEM containing 0.1 mM L012, 1 mM H_2O_2, 4 mM Im, 20 nM hemin-D1/D2-hemin, 20 nM hemin-D3/D4-hemin, 40 nM DNM, 20 ng mL^{-1} PCSK9-P1, 20 ng mL^{-1} Ab2-P2, 20 nM iblock/initiator and different concentrations of PCSK9-Ab. A total 75 data points were collected on microchip, outliers were determined and removed through Grubbs test, error bars: mean ± SD.

released initiator then triggered the DNM to produce a large number of primers, which finally turned on the hemin-DNA switch to generate CL signal. Using PCSK9-Ab as a model analyte, the assay time for PCSK9-Ab detection was optimized to be 30 min (Figure S17, Supporting Information), at which the CL intensity increased with the increasing logarithm of PCSK9-Ab concentration from 10 pg mL^{-1} to 1 ng mL^{-1} (Figure 3h).The limit of detection based on three times standard deviation was calculated to be 5.67 pg mL^{-1}, which was comparable to rolling circle amplification based homogenous fluorescent assay (1.11 pg mL^{-1})[20] and heterogenous colorimetric assay (2.82 pg mL^{-1})[21] for protein, and much lower than other assays based on HCR (39.6 pg mL^{-1}, 6 μg mL^{-1}, 1.76 mg mL^{-1}).[22–24] Using other mAbs as the targets, the specificity of the proposed CL assay was demonstrated (Figure 3i). The CL signal was observed only in the sample containing PCSK9-Ab.

2.5. Microchip for CL Immunoimaging of Single-Cell Secretion

In order to achieve CL immunoimaging of single-cell secretion, a microchip model comprising 25 units for cell capture and CL imaging was designed (**Figure** 4a). In this microchip, a series of polydimethylsiloxane (PDMS) cylindrical units were connected via two parallel channels, which were used for liquid or air injection (Figure S18a, Supporting Information). The diameter of each microwell was 200 μm, which provided the clear shape of the CL dot signal, and a 2 μm gap was designed for the cell capture. The width of two parallel channels was 35 μm and the height of the chip structure was set at 25 μm to ensure the smooth passage of cells through the chip (Figure S18b, Supporting Information). Based on these dimensions of the fabricated chip, the total volume of each reaction unit was calculated to be 0.79 nanoliter. The single cell loading in the microwells could be achieved on the designed microchip through the hydrodynamic differential flow resistance principle.[25]

The CL performance of both G4/hemin and hemin-DNA switch catalyzed Im-L012-H_2O_2 system were evaluated on the microchip. The CL dot signal of G4/hemin catalyzed Im-L012-H_2O_2 system could not be collected by CCD due to the flash-type CL emission (Figure 4b). In contrast, due to the strong and persistent CL emission of Im-enhanced hemin-DNA switch-L012-H_2O_2 system, the CL dot signal could be recorded in the presence of primer, which guaranteed the possibility of MCCLII protocol for in situ protein detection on microchip.

To assess the feasibility of the proposed MCCLII protocol on the designed microchip for antibody detection, different amounts of PCSK9-Ab were mixed with CL detection reagents and injected into the chip. After isolated each microwells with air to from microdroplet in each microchamber, the antibody-triggered DNM could be operated and the released primers activated hemin-DNA switch to produce strong CL signal confined in a microwell (Figure 4c). The CL dot signal exhibited a clear correlation with the concentration of PCSK9-Ab and could be distinctly identified even at the concentration down to 10 pg mL^{-1} (66 antibodies in 0.79 nL) (Figure 4d). When the concentration of PCSK9-Ab was

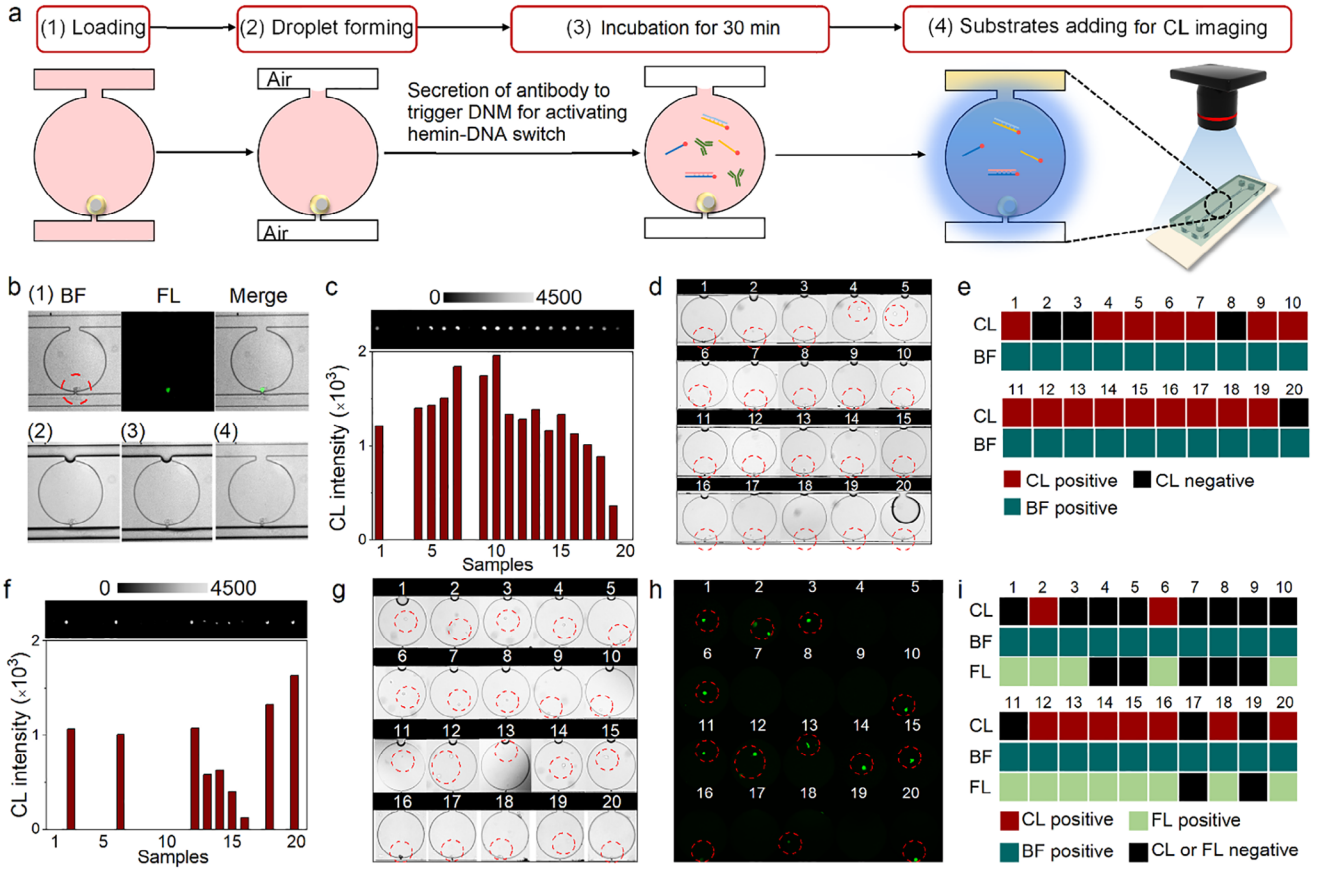

Figure 5. a) Schematic diagram of the workflow of MCCLII protocol for in situ detection of antibody secreted from single hybridoma cell. b) Microscopic images of single hybridoma cell captured in microcavity 1), formed microdroplet after air-cutting at 0 min 2), 30 min 3) and after adding CL substrates 4). c) CL images and intensities and d) bright field images obtained from 20 single PCSK9-6E3 hybridoma cell samples. e) Signal comparison of MCCLII results in c and microscopic results in d. f) CL images and intensities, g) bright field images and h) FL images obtained from 20 single cell samples. i) Signal comparison of MCCLII, microscopic and FL results in f-h.

higher than 1 ng mL^{-1}, the decreased CL signals could be attributed to the Hook effect.[26] Besides, the variability of CL intensity was noticed, which might resulted from the uneven droplets distribution in microfluidic operations. The operation error could be decreased by a skilled operator to further enhance the credibility of image-based detection. The box diagram of CL intensity versus PCSK9-Ab concentration exhibited linearity ranging from 0.01 to 1 ng mL^{-1} (Figure 4e). This sensitive lab-on-chip CL assay enabled the rapid in situ detection of antibody secreted from single hybridoma cells, which avoided a long incubation period on microfluidic chip and ensured the activity of screened cells for subsequent hybridoma cell culture.

2.6. In Situ Immunoimaging of PCSK9-Ab Secreted from 6E3 Hybridoma Cells on Microchip

The MCCLII protocol for in situ detection of PCSK9-Ab secreted from specific hybridoma cells on the microchip was illustrated in **Figure** 5a. First, hybridoma cells suspended in DMEM containing affinity probes, iblock/initiator, hemin-D1/D2-hemin, hemin-D3/D4-hemin and DNM were loaded into the chip for single cell capture (Figure 5b-1). Air was then introduced to form droplet in each microchamber (Figure 5b-2), followed with 30-min incubation, during which the antibody secreted from the specific hybridoma cells could trigger the DNM-regulated hemin-DNA switch to activate the hemin-DNA (Figure 5b-3). Afterward, the mixture of Im, L012 and H_2O_2 was gently injected the chambers (Figure 5b-4) to in situ collect the CL dot signals responding to specific hybridoma cells captured in the microwells with an exposure time of 1.5 min. The impact of CL substrates on hybridoma cells was evaluated by the CCK-8 kit (Figure S19, Supporting Information). Neither each reactant nor the mixture of CL substrates affected the activity of hybridoma cells, which ensured that hybridoma cells could continue to be cultured for specific antibody production.

The performance of the MCCLII for in situ detection of PCSK9-Ab secreted from single 6E3 hybridoma cells was evaluated by collecting the CL (Figure 5c) and bright field (BF) (Figure 5d) images of 20 single cell samples, which showed different CL imaging brightness due to the heterogeneity of hybridoma cells. The positive rate was calculated to be 80% (16 positive cells out of 20 samples, Figure 5e), and four samples of single 6E3 hybridoma cell were CL negative due to their low secretory activity. It should be noted that the initial concentration of the target antibody was relatively lower than the affinity probes loaded in

the microwell due to the insitu secretion of target antibody from single hybridoma cell, the CL assay could be free from the Hook effect in a short incubation time. According to the detction results, single 6E3 hybridoma cell could secrect 6 pg ng mL^{-1} – 0.4 ng mL^{-1} of the antibody in 30 min, which was much lower than the values reported previouly (calculated to be ng mL^{-1} to tens ng mL^{-1} level in 30 min)[4] based on a FL detection method without signal amplification. The possible reason might be that the proposed MCCLII protocol required 30-min incubation time for sustained secretion of antibody and the signal amplification, thus the detection results of secreted antibody during the 30-min incubation time were not the cumulative sum of secreted antibodies, but only the antibody secreted from hybridoma cell in the early stage. Thus, the MCCLII protocol could be used only for specific hybridoma cell screening.

2.7. Screening of Heterogeneous Hybridoma Cells

The screening capacity of the proposed MCCLII protocol for specific hybridoma cells was further verified on the designed microchip. After the positive PCSK9-6E3 hybridoma cells were stained with CellTracker Green CMFDA dye, which did not impact the secretory activity, they were mixed with NT-proBNP-3H1 hybridoma cells, and the mixed suspension was subsequently used to perform the screening of PCSK9-6E3 hybridoma cells. CL, BF and FL images of 20 single cell samples were shown in Figure 5f–h. The CL signals could be observed from the microwells capturing single PCSK9-6E3 hybridoma cells, which showed green dots, excluding the signal crosstalk between each microcavity. 9 positive samples were selected from 13 PCSK9-6E3 hybridoma cells, and all 7 negative samples were matched between CL and FL images (Figure 5i), indicating acceptable accuracy for specific hybridoma cell screening through lab-on-chip CL assay. 4 negative results of PCSK9-6E3 hybridoma cells could be attributed to their insufficient secretion ability. Therefore, the rapid and simple MCCLII protocol provided a promising microfluidic platform for the in situ detection of single cell secretion.

3. Conclusion

The heterogeneity of the secretory capacity of fused hybridoma cells is a primary limiting factor in hybridoma technology, thus the screening of specific antibody-secreting hybridoma cells with high secretory capacity is a crucial step to improve the efficiency of hybridoma technology In this study, we discover the CL enhancement of Im on hemin-DNA-L012-H_2O_2 system due to the coordination between Im and hemin moiety to improve the affinity of hemin moiety to L012, and the reduction of reaction energy to facilitate the hemin moiety-catalytic L012 oxidation, which lead to a strong and long-lasting CL emission, and thus develop a highly sensitive MCCLII protocol for efficient in situ detection of antibody secreted from single hybridoma cells on a microfluidic platform by using Im-assisted hemin-DNA-L012-H_2O_2 CL system and a DNM amplified hemin-DNA switch. Using PCSK9-Ab as a model analyte, the CL assay strategy shows a LOD of 5.67 pg mL^{-1} under 30 min incubation along with excellent specificity, and its application in improving the efficiency of hybridoma technology has been verified on a designed microchip with a single microchamber volume of 0.79 nL, which achieves the immunoimaging detection of 66 antibodies with short incubation period and acceptable accuracy. Moreover, the selected cells remain high antibody secretory activity. Due to the large area of the CL image captured by CCD, the high-throughput screening of hybridoma cells can be achieved by combining a multichannel flow injection system and multiple sets of microchips. Besides, by simply changing the affinity probes for the proximity binding-triggered DNM, the CL assay can be used for multiple targets detection, which further enhances the high-throughput detection of the proposed MCCLII protocol. However, the proposed MCCLII protocol is still limited by the Hook, and future work can set a built-in saturation warning in the microfluidic chip to improve the accuracy of the proposed CL assay. The long-term signal amplification strategy also limits the accurate quantitative detection of in situ secreted antibodies, thus CL assays without signal amplification need to be developed to achieve the accurate in situ detection of singel-cell secreted antibodies. In summary, The rapid and simple protocol possesses the advantages of convenient operation, low cost and good expansibility, and thus exhibits the potential application in the production of high-quality specific monoclonal antibody.

4. Experimental Section

Materials and Reagents: K_2HPO_4, KH_2PO_4, tris(2-carboxyethyl) phosphine hydrochloride (TCEP), 3-maleimidobenzoic N-hydroxysuccinimide ester (MBS), chloro-(protoporphyrinato) iron (III) (hemin), luminol, p-iodophenol (PIP), naphthol, L-histidine (His), 1,2,4-triazole (Tz), pyrazole (Pz), DMSO-d_6 and SYLGARD 184 silicone elastomer kit were purchased from Sigma–Aldrich Co. (Shanghai, China). 8-amino-5-chloro-2,3-dihydro-7-phenylpyrido-(3,4-d)-pyridazine-1,4-dione (L012) was purchased from Wako Pure Chemical Industries, Ltd (Osaka, Japan). Imidazole (Im), 2-methylimidazole (2-MIM), imidazole-2-carboxaldehyde (ICA) and 1-methyl-1H-imidazole-5-carboxaldehyde (MICA) were purchased from Aladdin Biochemical Technology Co., Ltd. (Shanghai, China). 4-Chlorothiophenol, 1,4-naphthalenedicarboxylic acid (1,4-NTPA), tryptophan and N-(4-aminobutyl)-N-ethylisoluminol (ABEI) were purchased from Beijing InnoChem Science & Technology Co. Ltd. (Beijing, China). 1H-benzotriazole (BZTA) and isoluminol were purchased from Meryer Biochemical Technology (Shanghai, China). Silicon wafer, photoresist SU8-3025 and its developer were obtained from MicroChem Co., Ltd. (USA). Human proprotein convertase subtilisin/kexin type 9 (PCSK9) protein, anti-PCSK9 antibody (PCSK9-Ab, mouse monoclonal antibody, clone nos. 6E3), PCSK9-6E3 hybridoma cells, anti-aminoterminal pro-brain natriuretic peptides antibody (NT-proBNP-Ab, mouse mAbs, clone nos. T6), NT-proBNP-3H2 hybridoma cells and anti-SARS-CoV-2 nucleocapsid protein antibody (SARS-CoV-2 NP-Ab, mouse mAbs, clone nos. 8B1) were supplied by FANTIBODY (Chongqing, China). Anti-α-fetoprotein antibody (AFP-Ab, mouse mAbs, clone nos. 9K5) and anti-carcinoembryonic antigen antibody (CEA-Ab, mouse mAbs, clone nos. 2H4) were purchased from Beijing Key-biotech Co. Ltd. (China). Anti-5-methylcytosine (5mC) antibody (5mC-Ab, rabbit mAbs, clone nos. RM231) and goat anti-mouse IgG (Ab2, clone nos. RM 104) were obtained from Abcam Trading Co. Ltd (Shanghai, China). Dulbecco's modified eagle medium (DMEM), BCA protein kit and TMB Kit were bought from KeyGEN BioTECH Corp. Ltd (Jiangsu, China). UltraPower DNA dye was purchased from BioTeke Biotechnology Co. (Beijing, China). CellTracker Green CMFDA dye, fetal bovine serum (FBS), HEPES buffer, sodium pyruvate, L-glutamine and PS (10 U mL^{-1} penicillin and 10 mg mL^{-1} streptomycin) were purchased from Thermo Fisher (Shanghai, China). Hemin labeled oligonucleotides were purchased from Takara Bio Inc. (Beijing, China), and other DNA oligonucleotides were obtained from Sangon Biotechnology Co. Ltd. (Shanghai, China). The DNA sequences were listed in Table S1

(Supporting Information). PBS-1 (10 mM, containing 2.8 mM KH_2PO_4, 7.2 mM Na_2HPO_4, pH 7.2) and PBS-2 (10 mM, containing 9.5 mM KH_2PO_4, 0.2 mM Na_2HPO_4, pH 5.5) were used for the synthesis of affinity probes. Ultrapure water from a Millipore water purification system (Milli-Q, Millipore) was used for all experiments.

Instruments: The CL imaging on 96-well plate was conducted with BioSpectrum 615 Imaging System. The CL micro-imaging was conducted with Tanon 5200 multi automatic chemiluminescence image analysis system. The CL signal was collected by the mean pixel intensity within a circle with VisionWorks imaging analytical system. Enzymatic activity and CL kinetic studies were performed on MPI-A analytical system (Xi'an Remex Analytical Instrument Co., Ltd. China). The colorimetric measurements were performed on Multiskan Sky (Thermo Fisher, USA). Absorption spectra was recorded on UV-3600 UV–vis-NIR spectrophotometer (Shimadzu Company, Japan). Fluorescence spectra was collected with Hitachi F-7000 fluorescence spectrophotometer (Hitachi, Japan). 1H NMR spectra was obtained on Bruker avanceIIIHD-500 spectrometer (Bruker, Germany) at 25 oC on 400 MHz. The gel electrophoresis analysis was performed on Mini-PROTEAN Tetra System (Bio-RAD, USA) and imaged on Biorad ChemDoc XRS (Bio-Rad, USA). The photolithography was carried out on a pattern conversion and nano imprint system (SUSS, Germany). Oxygen plasma treatment of glass and PDMS were conducted with Plasma cleaner PDC-002 (Harrick, USA).

Preparation of DNM and Affinity Probes: DNM was obtained through the assembly of C1 and C2 on DNA skeleton with a linker. C1 and C2 were synthesized by mixing block-1 and primer-1 or block-2 and primer-2 at a ratio of 1:1 and remaining at 95 °C for 5 min, which were cooled to room temperature naturally. Afterword, 10 µL of 10 µM C1 and 10 µL of 10 µM C2 were mixed with 10 µL of 10 µM linker, 5 µL of 10 µM DNA skeleton and 15 µL PBS-1 for 30 min at 37 °C for the assembly of DNM.

After separately mixing PCSK9 and Ab2 (20 µL, 2 mg mL^{-1}) with MBS (40 µL, 0.2 mg mL^{-1}) and 140 µL PBS-1 at room temperature for 2 h, then filtrating for 8 times (30 kDa, 8000 rpm, 5 min) to obtain the complexes, and separately mixing thiolated DNAs (P1 and P2, 10 µL, 100 µM) with TCEP (30 µL, 5 mM) and 150 µL PBS-2 at room temperature for 2 h, then filtrating for 5 times (10 kDa, 12 000 rpm, 10 min) to obtain reduced P1 and P2, the affinity probes were prepared by mixing the reduced P1with PCSK9-MBS complex, and the reduced P2 with Ab2-MES complex to incubate at room temperature for 2 h, and then purifying the products by ultrafiltration (50 kDa, 8000 rpm, 5 min) for 8 times. The obtained affinity probes were stored at −20 °C, and their concentrations were calibrated with BCA protein assay kits.

Chip Fabrication: The silicon mold for cell capturing and CL imaging was produced by photolithography. Briefly, the photoresist was flatted on a silicon wafer with 25 µm height and solidified by sequentially heating at 65 °C (1 min), 95 °C (5 min), and 65 °C (1 min). The mask with designed structure was covered on the obtained solidified silicon wafer for 4.5 s exposure under ultraviolet light in a photoetching machine. The silicon wafer with designed pattern was obtained by baking at 90 °C for 30 min, alternately developing in developer and isopropanol, and then heating at 180 °C for 30 min. PDMS precursor solution was obtained by thoroughly stirring the mixture of polydimethylsiloxane and curing agent at a ratio of 10:1, and removing bubbles with a vacuum pump. The silicon wafer with formed structure was then immersed in the PDMS precursor solution and cured at 85 °C for 30 min. The PDMS with pattern was cut and peeled off from the silicon wafer. Four holes were punched on the PDMS structure for inlets and outlets with a 1.5 mm puncher. The final chip was fabricated by bonding the PDMS structure on a glass after oxygen plasma treatment. The chip was immersed in DMEM before use.

Measurements of Hemin-DNA Catalytic Activity: Colorimetric and CL methods were used to evaluate the activity of hemin-DNA with different substrates in the absence and presence of Im, respectively. Different concentrations of TMB or L012 substrate were added into the mixture of 20 nM hemin-DNA, 1 mM H_2O_2 and 4 mM Im. The time-dependent absorbance at 418 nm or CL intensity was monitored for 10 min, respectively. The Lineweaver-Burk plots were used to calculate the Michaelis constant K_m and v_{max}.

Computational Methods: All calculations were carried out with the Gaussian 16 program.[27] The initial model of the reactants, intermediates, and final products involved in the initial reaction was structurally optimized with the B3LYP-D3 functional[28,29] and the 6–311G(d,p) basis set[30] in water (polarizable continuum model (PCM)[31,32] with SMD-coulomb atomic radii). For the corresponding product, the transition state had only an imaginary frequency, and the reactants, intermediates, and products had not imaginary frequency. The transition state was followed by the TS method in two directions following the intrinsic reaction coordinate (IRC) analysis to ensure that the transition state was related to the correct reactants and products. Frequency analysis and IRC analysis were performed using the same basis set as the optimization.

Electrophoresis Analysis: 8% native polyacrylamide gel was prepared using 1 × TBE buffer to load the mixtures, which were prepared by mixing 4 µL samples with 1 µL 6 × loading buffer and 1 µL UltraPowerTM DNA dye for 3 min. The gel electrophoresis was run at 100 V for 30 min in 1 × TBE buffer and visualized by BioSpectrum 615 Imaging System.

CL Response to Initiator: Hemin-D1/D2-hemin and hemin-D3/D4-hemin were obtained by mixing hemin-D1 and hemin-D2 or hemin-D3 and hemin-D4 at a ratio of 1:1 to incubate at 95 °C for 5 min and cooling the mixtures to room temperature. 1 µL initiator at different concentrations was mixed with DNM (2 µL, 1 µM), hemin-D1/D2-hemin (1 µL, 1 µM), hemin-D3/D4-hemin (1 µL, 1 µM) and DMEM (5 µL, pH 7.2) to incubate at 37 °C for 20 min. Then 40 µL CL substrate containing 0.125 mM L012, 5 mM Im and 1.25 mM H_2O_2 was added to perform the CL measurement with an exposure time of 30 s.

CL Response to PCSK9-Ab: 1 µL PCSK9-Ab at different concentrations was first added into 9 µL solution containing affinity probes PCSK9-P1 (1 µL, 1 µg mL^{-1}), Ab2-P2 (1 µL, 1 µg mL^{-1}), iblock/initiator (1 µL, 2 µM), hemin-D1/D2-hemin (1 µL, 1 µM), hemin-D3/D4-hemin (1 µL, 1 µM), DNM (2 µL, 1 µM) and DMEM (2 µL, pH 7.2) to incubate for 30 min at 37 °C. Afterward, 40 µL CL substrate containing 0.125 mM L012, 5 mM Im and 1.25 mM H_2O_2 was added to perform the CL measurement with an exposure time of 30 s.

Assay of PCSK9-Ab on Chip: PCSK9-Ab was diluted to different concentrations with DMEM. After 13 µL PCSK9-Ab sample was mixed with 7 µL solution containing affinity probes (2 µL, 1 µg mL^{-1}), iblock/initiator (1 µL, 2 µM), hemin-D1/D2-hemin (1 µL, 1 µM), hemin-D3/D4-hemin (1 µL, 1 µM) and DNM (2 µL, 1 µM), the mixture was introduced into the microchip immediately with a microinjection pump (10 µL min^{-1}) to fill the chambers of microchip, and then form the droplet in each microwell through air injection. After incubation for 30 min, 30 µL CL substrate containing 0.125 mM L012, 5 mM Im and 1.25 mM H_2O_2 was gently injected into the microchip from inlet1 to outlet1 to collect the CL images by CCD with an exposure time of 1.5 min.

In Situ Detection of Secreted PCSK9-Ab: PCSK9-6E3 and NT-proBNP-3H2 hybridoma cells were supplied by FANTIBODY (Chongqing, China). They were cultured in DMEM supplemented with 20% FBS, 0.1 mg mL^{-1} streptomycin, and 0.1 mg mL^{-1} penicillin at 37 °C in a humidified atmosphere containing 5% CO_2. After PCSK9-6E3 hybridoma cells were gently washed for 8 times, directly blown off with pipette and resuspended in DMEM containing affinity probes (0.1 µg mL^{-1}), iblock/initiator (0.1 µM), hemin-D1/D2-hemin (50 nM), hemin-D3/D4-hemin (50 nM) and DNM (0.1 µM). The resuspended cell suspension (1.79×10^4 cell mL^{-1}) was injected into a DMEM presoaked microchip, which was pre-vacuumed by a pump, the injection rate was 1 µL min^{-1}, and the single cell capture status was confirmed by a bright-field microscopy. The cell-contained droplets in microwells were formed in 1 min through the air injection (1 µL min^{-1}). After incubation for 30 min, 30 µL CL substrate containing 0.125 mM L012, 5 mM Im and 1.25 mM H_2O_2 was gently injected into the microchip from inlet1 to outlet1, to collect CL images by CCD with an exposure time of 1.5 min.

For confirming the feasibility of the proposed MCCLII protocol to screen specific hybridoma cells, the model sample of heterogeneous hybridoma cells was prepared by mixing the Cell Tracker Green CMFDA dye pre-stained PCSK9-6E3 hybridoma cells and non-stained NT-proBNP-3H2 hybridoma cells at a ratio of 1:1.

Statistical Analysis: For CL assay in 96-well plate, the CL signal was pre-processing using the VisionWorks imaging analytical system for background removal. Specifically, after the CL image collection, background removal was performed by substrating the CL signal of empty plate. Three images of each sample were collected, processed through the same steps, and the avereged data of each sample were used for further analysis. For CL microimaging analysis, a sample without target was first detected, and its mean intensity was calculated to be the background. Subsequently, the data pre-processing of each microwell of other sample was performed by subtracting the background.

For quantitative analysis of CL imaging assay proposed in this work, the CL signal of a reference sample was collected together with samples to be tested, after the backgound removal, each data was normalized according to the data of the reference sample. Each data was presented with its mean pixel intensity, and the error bar was calculated through three standered deviation. The sample size of each experiment was disicribed in the corresponding figure legend.

As for the CL assay of antibodies on the microchip, the image data of each microwell were conducted through the suspicious value determination via Grubb's test. Under the conditions of 25 samples, significance level of 0.05 and the confidence level of 90%, the data with calculated G value higher than the critical value should be delected.

The one-sided testing was used for the screening of specific hybridoma cells, the hybridoma cells with a CL signal higher than the background were identified as the positive sample. Origin was used for statistical analysis.

Supporting Information

Supporting Information is available from the Wiley Online Library or from the author.

Acknowledgements

This work was financially supported by the National Natural Science Foundation of China (21827812, 21635005, 21890741), Frontier Technology Research and Development Program of Jiangsu Province (BF2024055), and the Independent Research Foundation from State Key Laboratory of Analytical Chemistry for Life Science (5431ZZXM24010).

Conflict of Interest

The authors declare no conflict of interest.

Author Contributions

H.A. and W.X. contributed equally to this work. H.J. and J.W. initiated the project and were corresponding authors of this work. H.A. and J.W. conceived the study under the guidance of H.J. Manuscript was written through contributions of H.A., J.W., and H.J. H.A. and W.X. performed the experiments. H.A., W.X., and J.W. performed data analysis. W.C. and W.H. participated in manuscript reversion. All authors have given approval to the final version of the manuscript.

Data Availability Statement

The data that support the findings of this study are available from the corresponding author upon reasonable request.

Keywords

biosensors, chemiluminescence, cellular secretion, microfluidics, single-cell analysis

Received: April 3, 2025
Revised: June 11, 2025
Published online:

[1] a) A. Beck, T. Wurch, C. Bailly, N. Corvaia, *Nat. Rev. Immunol.* **2010**, *10*, 345; b) C. Dumontet, J. M. Reichert, P. D. Senter, J. M. Lambert, A. Beck, *Nat. Rev. Drug Discovery* **2023**, *22*, 641.
[2] a) G. Köhler, C. Milstein, *Nature* **1975**, *256*, 495; b) P. Chiarella, V. M. Fazio, *Biotechnol. Lett.* **2008**, *30*, 1303.
[3] Z. Chen, J. J. Chen, R. Fan, *Annu. Rev. Anal. Chem.* **2019**, *12*, 431.
[4] a) A. Jin, T. Ozawa, K. Tajiri, T. Obata, H. Kishi, A. Muraguchi, *Nat. Protoc.* **2011**, *6*, 668; b) B. E. Debs, R. Utharala, I. V. Balyasnikova, A. D. Griffiths, C. A. Merten, *Proc. Natl. Acad. Sci.* **2012**, *109*, 11570; c) L. Mazutis, J. Gilbert, W. L. Ung, D. A. Weitz, A. D. Griffiths, J. A. Heyman, *Nat. Protoc.* **2013**, *8*, 870; d) K. Eyer, R. C. L. Doineau, C. E. Castrillon, L. Briseño-Roa, V. Menrath, G. Mottet, P. England, A. Godina, E. Brient-Litzler, C. Nizak, A. Jensen, A. D. Griffiths, J. Bibette, P. Bruhns, J. Baudry, *Nat. Biotechnol.* **2017**, *35*, 977.
[5] a) M. Yang, J. Huang, J. Fan, J. Du, K. Pu, X. Peng, *Chem. Soc. Rev.* **2020**, *49*, 6800; b) K. Suzuki, T. Nagai, *Curr. Opin. Biotechnol.* **2017**, *48*, 135; c) X. Li, C. Yin, S. S. Liew, C. S. Lee, K. Pu, *Adv. Funct. Mater.* **2021**, *31*, 2106154; d) Z. Yu, H. Gong, Y. Li, J. Xu, J. Zhang, Y. Zeng, X. Liu, D. Tang, *Anal. Chem.* **2021**, *93*, 13389.
[6] a) Q. Xiao, C. Xu, *Trac-Trends Anal. Chem.* **2020**, *124*, 115780; b) W. Wu, B. T. T. Nguyen, P. Y. Liu, G. Cai, S. Feng, Y. Shi, B. Zhang, Y. Hong, R. Yu, X. Zhou, A. Q. Liu, Y. Zhang, E. P. H. Yap, L. K. Chin, *Biosens. Bioelectron.* **2022**, *215*, 114594; c) S. Chen, J. Zhao, C. Xu, I. Y. Sakharov, S. Zhao, *Anal. Chem.* **2021**, *93*, 9218; d) D. Yang, Y. Fang, X. Liu, J. Ma, J. Xu, H. Dong, H. Ding, D. Wang, Q. Liu, F. Zhang, *Nano Lett.* **2024**, *24*, 14875.
[7] a) S. Liu, J. Li, Y. Zou, Y. Jiang, L. Wu, Y. Deng, *Small* **2023**, *19*, 2304631; b) Q. Xiao, J. Wu, P. Dang, H. X. Ju, *Anal Chim. Acta.* **2018**, *1032*, 130.
[8] a) E. M. McConnell, I. Cozma, Q. Mou, J. D. Brennan, Y. Lu, Y. Li, *Chem. Soc. Rev.* **2021**, *50*, 8954; b) J. Yan, M. Ran, X. Shen, H. Zhang, *Adv. Mater.* **2023**, *35*, 2300374; c) Z. Yu, Z. Xu, R. Zeng, M. Xu, H. Zheng, D. Huang, Z. Weng, D. Tang, *Angew. Chem., Int. Ed.* **2025**, *64*, 20241462. d) Z. Yu, J. Tang, H. Gong, Y. Gao, Y. Zeng, D. Tang, X. Liu, *Adv. Funct. Mater.* **2023**, *33*, 2301457.
[9] a) J. Xu, R. Jiang, H. He, C. Ma, Z. Tang, *Trac-Trends Anal. Chem.* **2021**, *139*, 116257; b) R. Zhang, J. Wu, H. Ao, J. Fu, B. Qiao, Q. Wu, H. X. Ju, *Anal. Chem.* **2021**, *93*, 9933; c) H. Ao, W. Xiao, Y. Chen, J. Wu, H. X. Ju, *Sens. Actuator B-Chem.* **2023**, *383*, 133579.
[10] a) R. Golnak, J. Xiao, K. Atak, M. Khan, E. Suljoti, E. F. Aziz, *J. Phys. Chem. B.* **2015**, *119*, 3058; b) A. M. Alsharabasy, A. Pandit, P. Farràs, *Adv. Mater.* **2021**, *33*, 2003883.
[11] a) Q. B. Wang, N. Xu, Z. Gui, J. Lei, P. Ju, X. H., F. Yan, *Chem. Commun.* **2014**, *50*, 15362; b) Q. B. Wang, N. Xu, Z. Gui, J. Lei, P. Ju, X. H., F. Yan, *Analyst* **2015**, *140*, 6532.
[12] a) Z. Dong, S. Xia, A. M. A. Alboull, I. M. Mostafa, A. Abdussalam, W. Zhang, S. Han, G. Xu, *ACS Appl. Nano Mater.* **2024**, *7*, 2983; b) W. R. Hu, H. Ao, Z. Y. Lv, W. Xiao, W. Li, J. Lei, J. Wu, H. Ju, *Anal Chim. Acta.* **2024**, *1328*, 343182.
[13] a) P. Jones, H. B. Dunford, *J. Inorg. Biochem.* **2005**, *99*, 2292; b) R. N. Samajdar, D. Manogaran, S. Yashonath, A. J. Bhattacharyya, *Phys. Chem. Chem. Phys.* **2018**, *20*, 10018; c) X. Zhang, D. Qiu, J. Chen, Y. Zhang, J. Wang, D. Chen, Y. Liu, M. Cheng, D. Monchaud, J.-L. Mergny, H. Ju, J. Zhou, *J. Am. Chem. Soc.* **2023**, *145*, 4517.
[14] S. Nakayama, J. Wang, H. O. Sintim, *Chem. - Eur. J.* **2011**, *17*, 5691.
[15] A. Chatterjee, C. Mahato, D. Das, *Angew. Chem., Int. Ed.* **2021**, *60*, 202.
[16] T. B. Nguyen, L. Ermolenko, M. E. T. H. Dau, A. Al-Mourabit, *Heterocycles* **2014**, *88*, 403.

[17] a) J. Zielonka, J. D. Lambeth, B. Kalyanaraman, *Free Radical Bio. Med.* **2013**, *65*, 1310; b) M. Tan, Y. Wang, Z. Hong, P. Zhou, J. Jiang, B. Su, *Analyst* **2024**, *149*, 1496.
[18] T. Min, J. C. Fettinger, A. K. Franz, *ACS Catal.* **2012**, *2*, 1661.
[19] H. Zhang, F. Li, B. Dever, X. F. Li, X. C. Le, *Chem. Rev.* **2013**, *113*, 2812.
[20] X. Luo, J. Zhao, X. Xie, F. Liu, P. Zeng, C. Lei, Z. Nie, *Anal. Chem.* **2020**, *92*, 16314.
[21] M. You, P. Peng, Z. Xue, H. Tong, W. He, P. Mao, Q. Liu, C. Yao, F. Xu, *Analyst* **2021**, *146*, 2871.
[22] F. Qiu, X. Gan, B. Jiang, R. Yuan, Y. Xiang, *Sens. Actuator B-Chem.* **2021**, *331*, 129395.
[23] X. Xue, M. Zhang, S. Hajizadeh, P. O. Larsson, L. Ye, *ACS Appl. Polym. Mater.* **2023**, *5*, 680.
[24] N. Li, L. Liu, M. H. Xiang, J. W. Liu, R. Q. Yu, J. H. Jiang, *Chem. Commun.* **2019**, *55*, 4387.
[25] a) M. Zhang, Y. Zou, X. Xu, X. Zhang, M. Gao, J. Song, P. Huang, Q. Chen, Z. Zhu, W. Lin, R. N. Zare, C. Yang, *Nat. Commun.* **2020**, *11*, 2118; b) N. N. Wang, H. Ao, W. C. Xiao, W. W. Chen, G. M. Li, J. Wu, H. X. Ju, *Biosens. Bioelectron.* **2022**, *201*, 113959.
[26] W. Chen, S. Shan, J. Peng, D. Liu, J. Xia, B. Shao, W. Lai, *Sens. Actuator B-Chem.* **2020**, *321*, 128465.
[27] M. J. Frisch, G. W. Trucks, H. B. Schlegel, *Gaussian 16, revision C.01* **2016**, Gaussian Inc., Wallingford CT, https://gaussian.com/citation.
[28] S. Grimme, J. Antony, S. Ehrlich, H. Krieg, *J. Chem. Phys.* **2010**, *132*, 154104.
[29] C. Lee, W. Yang, R. G. Parr, *Phys. Rev. B.* **1988**, *37*, 785.
[30] A. D. McLean, G. S. J. Chandler, *J. Chem. Phys.* **1980**, *72*, 5639.
[31] S. Miertuš, E. Scrocco, J. Tomasi, *Chem. Phys.* **1981**, *55*, 117.
[32] J. Tomasi, B. Mennucci, R. Cammi, *Chem. Rev.* **2005**, *105*, 2999.